Acta Astronautica Vol. 13, No. 6/7, pp. 301–309, 1986
Printed in Great Britain.

0094-5767/86 $3.00 + 0.00

ATTITUDE PERTURBATIONS INDUCED BY FREE-MOLECULAR FLOW INTERACTIONS IN PERIGEE REGION†

JOZEF C. VAN DER HA‡
E.S.A., European Space Operations Centre, Robert-Bosch-Strasse 5, 6100 Darmstadt, F.R.G.

(*Received* 14 *January* 1986)

Abstract—A theoretical model for the spin axis attitude changes induced by free-molecular torques during the perigee region passage in a geostationary transfer orbit is developed. It is shown that the direction of the attitude change is essentially normal to the plane formed by the attitude orientation and perigee velocity vector. A verification of the model is performed using actual Marecs-A solar aspect angle measurements before and after the three perigee passages. A consistency of better than 16% is achieved between predicted and reconstituted attitude changes. The discrepancies between the results for the three perigee passages are expected to be due to deficiencies in local air density modelling.

1. INTRODUCTION

All ESA geostationary satellites launched so far have been spin-stabilised during Apogee Motor Firing (AMF). Spin-stabilisation is a convenient mode for providing sufficient inertial pointing stability during the AMF phase without having to resort to active attitude control torques.

Since the satellite's spin axis orientation defines the direction of the change in orbit velocity during Apogee Motor Firing, an offset of the spin axis orientation from the optimal one has a direct impact on the achieved near-geostationary orbit. Such injection errors usually need to be corrected by means of fuel which otherwise would be available for normal-mode attitude and orbit control objectives. Hence it is of utmost importance to reduce attitude orientation errors at AMF to the minimum possible thereby effectively increasing the satellite's useful lifetime. This can be achieved by ensuring that attitude estimation procedures make optimal use of the available sensor data. On the other hand, a detailed assessment of all possible attitude changes during the transfer orbit phase needs to be performed. Concentrating now on attitude effects produced by the space environment in a typical transfer orbit it is found that torques induced by the free-molecular flow in the perigee region are dominant. Ariane-launched satellites have their perigees near 200 km altitude which means that free-molecular effects are appreciable only for perhaps 15 min around the perigee passage time.

The present paper analyses the free-molecular interactions with the spacecraft for the prevailing air density conditions in the perigee region. A detailed model is derived for the momentum interactions governing the magnitude and direction of the torque vector as a function of orbital eccentric anomaly. An analytical integration of the torque vector over the relevant perigee region is carried out with the aid of an asymptotic method. It is shown that the effect of the integrated torque may be interpreted as an instantaneous attitude change at perigee in a direction essentially normal to the plane formed by the perigee velocity and spin axis attitude vectors.

The model constructed has been subjected to in-orbit verification using actual sensor data of ESA's Marecs-A satellite launched by an Ariane rocket on 20 December 1981. It is fortunate that the attitude change could be made visible after filtering of the solar aspect angle measurements. Since these are the only attitude-related measurements available in the perigee region only one component of the predicted attitude change is actually observable. By relying on the predicted torque direction, however, it becomes possible to compare predicted and observed attitude changes. These are shown to be of the order of 0.05° in the case of Marecs-A. The agreement between predicted and observed values is reasonably good considering the uncertainty in local air density characteristics.

2. GENERAL FREE-MOLECULAR TORQUE MODEL

2.1. *Torque expressions for idealised satellite configurations*

The interaction of the free-molecular flow with a spinning satellite surface results in torques affecting the satellite's attitude orientation. In a previous paper (Van der Ha[1]) expressions for the torques induced by the free-molecular flow have been established for a few idealised spinning satellite configurations. The

†Paper presented at the *36th Congress of the International Astronautical Federation*, Stockholm, Sweden, 7–12 October, 1985.

‡Senior Analyst.

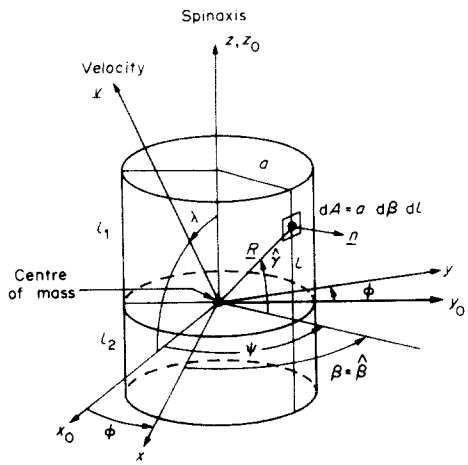

Fig. 1. Geometry of a cylinder satellite configuration.

expression for the free-molecular torque on a cylindrical shell can be formulated as follows

$$\mathbf{M}_c = -\tfrac{1}{2}\rho v^2 a\,(l_1 + l_2)\{(l_1 - l_2)[c_0 + (\pi/4)c_1 \sin\lambda + \tfrac{1}{3}(2c_2 + c_3)\sin^2\lambda] - (a\pi/4)c_3 \sin(2\lambda)\}\,\mathbf{y}_0 \quad (1)$$

Here ρ stands for the local air density and v for the satellite's orbital velocity. The geometrical parameters a, l_i $(i = 1, 2)$ can be visualised from Fig. 1. The direction of the torque is along the direction of y_0, i.e. normal to the plane formed by the spin axis z and velocity vector $\mathbf{v}$. The x_0 axis is defined such that the velocity vector $\mathbf{v}$ lies in the x_0, z_0 plane. The angle of incidence from the z axis lies thus between 0 and 180°. Finally, the "accommodation parameters" c_j $(j = 0, \ldots, 3)$ are defined by

$$c_0 = (2 - \sigma_n)(v_m/v)^2, \quad c_1 = \sigma_n\sqrt{\pi}\, v_w/v, \quad c_2 = 2(2 - \sigma_n), \quad c_3 = 2\sigma_t \quad (2)$$

where v_m, v_w designate the most probable thermal speeds of the molecules at ambient atmospheric and surface temperatures, respectively.

The normal and transverse accommodation coefficients σ_n, σ_t represent the extent of adaptation to surface conditions before the molecules are reemitted: when σ_n and σ_t are close to 1 virtually all molecules are completely accommodated so that reemission takes place with a velocity v_w determined by the surface temperature. If σ_n and σ_t are close to zero, virtually all molecules are reflected specularly without accommodation. In most practical applications the coefficients σ_n and σ_t lie between 0.9 and 1. Physically, one may interpret the parameters in eqn (2) as follows,

c_0: normal momentum transfer of incident and specularly reflected molecules due to thermal speed.
c_1: normal momentum transfer of molecules reemitted after accommodation at surface temperature.
c_2: normal momentum transfer of incident and specularly reflected molecules due to orbital speed.
c_3: transverse momentum transfer of incident molecules which are not specularly reflected.

Depending on the sign of $\pi/2 - \lambda$, either the top or bottom of a cylindrical satellite will also be subjected to free-molecular momentum interactions. The resulting torque can be formulated as

$$\mathbf{M}_0 = -(\pi/4)\rho v^2 a^2 l_i c_3 \sin(2\lambda)\,\mathbf{y}_0 \quad (3)$$

with $i = 1$ or 2 when $\pi/2 - \lambda$ is positive or negative.

The free-molecular flow induced torque on a box-like satellite can be expresses as (Van der Ha[1])

$$\mathbf{M}_b = -\rho v^2\{(A_1 + A_2)(R_z/\pi)[c_0 + (\pi/4)c_1 \sin\lambda + \tfrac{1}{3}(2c_2 + c_3)\sin^2\lambda] + \tfrac{1}{8}(2A_0 R_0 - A_1 R_x - A_2 R_y)c_3 \sin(2\lambda)\}\,\mathbf{y}_0 \quad (4)$$

It may be mentioned that R_0 refers to the distance to the "bottom" surface in the case that $\lambda > \pi/2$. It can be checked that the contribution due to A_0 given in eqn (4) is identical to the expression of eqn (3) when $A_0 = \pi a^2$ is substituted. It must be kept in mind that the distances R_0, R_x and R_y are defined to be always positive, whereas R_z becomes negative when the centre of mass would lie above the geometrical centre of the side surfaces.

On the basis of the expressions given above for the two most common satellite configurations a general torque model of the form

$$\mathbf{M} = -\rho v^2\{b_0 + b_1 \sin\lambda + b_2 \sin^2\lambda + \tfrac{1}{2}b_3 \sin(2\lambda)\}\,\mathbf{y}_0 = -\rho\,(\mathbf{z}\times\mathbf{v})\{b_0 v^2/|\mathbf{z}\times\mathbf{v}| + b_1 v + b_2|\mathbf{z}\times\mathbf{v}| + b_3(\mathbf{z}\cdot\mathbf{v})\} \quad (5)$$

is postulated. Table 1 summarises the resulting coefficients b_j $(j = 0, \ldots, 3)$ for the box-like and cylindrical satellites (including top or bottom surfaces) presented above.

2.2. *Marecs-A torque model*

In order to obtain a feeling for the relative importance of the various contributions to the torque

Table 1. Coefficients b_j for idealised satellite configurations (the $\pm$ sign refers to sign of $\pi/2 - \lambda$)

Coefficient	Box	Cylinder
b_0	$R_z(A_1 + A_2)c_0/\pi$	$a(l_1^2 - l_2^2)c_0/2$
b_1	$R_z(A_1 + A_2)c_1/4$	$a(l_1^2 - l_2^2)\pi c_1/8$
b_2	$R_z(A_1 + A_2)(2c_2 + c_3)/(3\pi)$	$a(l_1^2 - l_2^2)(2c_2 + c_3)/6$
b_3	$(2A_0 R_0 - A_1 R_x - A_2 R_y)c_3/4$	$\pm a^2(l_1^2 - l_2^2)\pi c_3/4$

model introduced above the particular values for the Marecs-A satellite during its Transfer Orbit are substituted. The inertial positions of its three perigee crossings had a local solar time near midnight. According to information from density models (Stickland[2]) the ambient atmospheric temperature must have been close to 1000 °K. This would result in a most probable thermal speed of the molecules of about $v_m = 950$ m/s. Ths speed ratio v_m/v can be taken equal to 0.093 to an accuracy of better than 2% within the relevant 200 km altitude region above perigee. On the basis of a surface temperature in the neighbourhood of 300 K the speed ratio v_w/v of the reemitted molecules after accommodation can be obtained with the aid of kinetic gas theory

$$v_w/v = (T_w/T)^{1/2}(v_m/v) = 0.051 \tag{6}$$

The Marecs-A satellite may be approximated by a box with dimensions

$$R_x = R_y = 0.809\text{ m};\quad R_z = 0.215\text{ m};\quad R_0 = 0.762\text{ m};$$
$$A_1 = A_2 = 3.16\text{ m}^2;\quad A_0 = 2.62\text{ m}^2 \tag{7}$$

It should be noted that R_0 points to the "bottom" surface (Fig. 2) since the angle of incidence λ is near 162° over the perigee region. The coefficients b_j ($j = 0, \ldots, 3$) defined in Table 1 become now (on basis of $\sigma_n = \sigma_t = 0.9$)

$$b_0 = 4.1 \times 10^{-3};\quad b_1 = 2.8 \times 10^{-2};$$
$$b_2 = 0.89;\quad b_3 = -0.50 \tag{8}$$

For the Marecs-A value of $\lambda = 162°$ the b_3 term is responsible for the largest contribution in eqn (5) followed by b_2 (about 58% of b_3 contribution), b_1 (about 6%) and b_0 (about 3%).

The behaviour of the resulting torque given in eqn (5) as a function of the angle of incidence λ is illustrated in Fig. 3 on the basis of Marecs-A parameters. The relative insensitivity of the torque to uncertainties in the accommodation coefficients is demonstrated by the two different cases ($\sigma_n = \sigma_t = 1$ and 0.9). The behaviour of the torque as a function of λ may roughly be interpreted as follows. For values of λ up to about 30° the transverse momentum transfer on the side surfaces is dominant: this leads to a small torque about the positive y_0 axis. For values

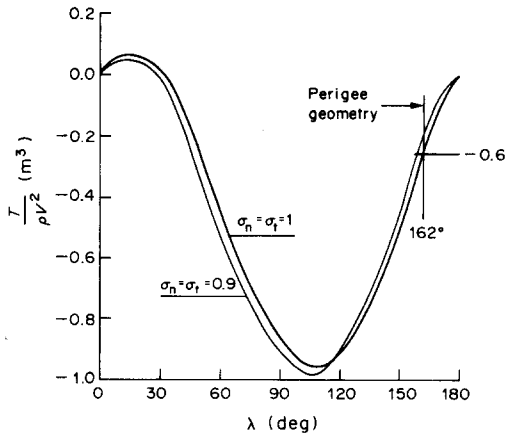

Fig. 3. Variation of torque as function of angle of incidence for Marecs-A parameters.

of λ above 30° of normal momentum transfer on the side surfaces becomes important resulting in an increasing torque about the negative y_0 axis. This trend is enforced by the fact that the transverse torque component on the top surface increases whereas that on the side surfaces decreases. For λ above 90° the bottom surface becomes effective with a transverse torque component acting along the $+y_0$ direction. However, since R_0 is smaller now the transverse torque due to the side surfaces more than balances this effect so that the resulting torque (which includes also the normal component on the side surfaces) remains along the negative y_0 axis until λ approaches 180°.

2.3. *Torque expression in eccentric anomaly*

In order to prepare for the integration of the torque over the perigee region it is necessary to express the general torque expression of eqn (5) in terms of the eccentric anomaly E. The orbital velocity expression in terms of E is

$$\mathbf{v}(E) = \sqrt{\mu/a}$$
$$\times \{-\sin E\,\boldsymbol{\xi}_p + s\cos E\,\boldsymbol{\eta}_p\}/(1 - e\cos E) \tag{9}$$

with $s = (1 - e^2)^{1/2}$; a is the semimajor axis, and μ the Earth's gravitational parameter. The unit-vectors $\boldsymbol{\xi}_p$ and $\boldsymbol{\eta}_p$ are part of the local orbital reference frame at perigee (Fig. 4). The transformation between this

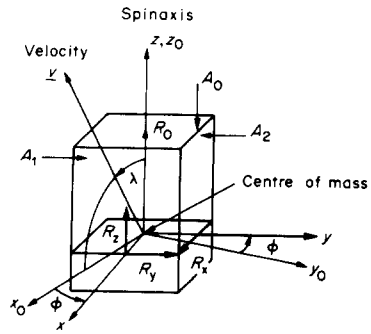

Fig. 2. Geometry of a box-like satellite configuration.

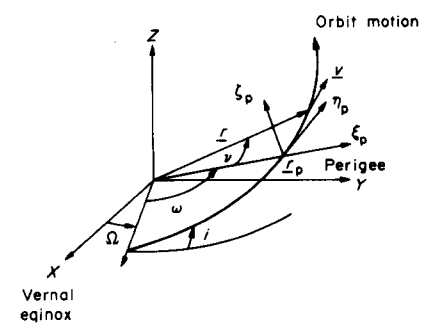

Fig. 4. Geometry of perigee reference frame.

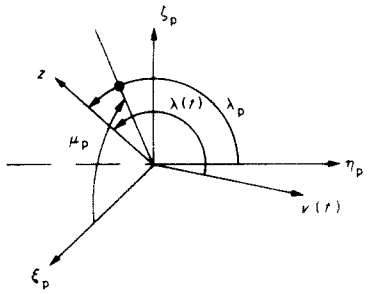

Fig. 5. Definition of cone and clock angles λ_p, μ_p.

frame and the inertial X, Y, Z frame is well known in terms of the orbital elements Ω, ω, and i and does not need to be repeated here. The magnitude of the velocity vector in eqn (9) is given by

$$v(E) = \sqrt{\mu/a}\,\{(1 + e\cos E)/(1 - e\cos E)\}^{1/2} \quad (10)$$

The air density as a function of eccentric anomaly is represented by the King–Hele[3] model

$$\rho(E) = \rho_p \exp\{-(r - r_p)/H_p\} = \rho_p \exp\{-\beta(1 - \cos E)\} \quad (11)$$

where ρ_p and H_p designate the reference air density and scale height both evaluated at perigee. The parameter β is defined by

$$\beta = ae/H_p \quad (12)$$

which is of the order of 500 for typical transfer orbit conditions. It can be seen from eqn (11) that for $E = \pm 8°$ the density is already below 1% of that at perigee. The region $-8° < E < 8°$ corresponds to a total interval in true anomaly of 40° and lasts only some 7.5 min.

The reference spin axis orientation may be considered fixed in inertial space. Its components along the perigee frame introduced above are constants which can conveniently be expressed in terms of the cone and clock angles λ_p, μ_p (Fig. 5)

$$\mathbf{z} = z_1\boldsymbol{\xi}_p + z_2\boldsymbol{\eta}_p + z_3\boldsymbol{\zeta}_p \quad (13)$$

with

$$z_1 = \sin\lambda_p\cos\mu_p, \quad z_2 = \cos\lambda_p, \quad z_3 = \sin\lambda_p\sin\mu_p \quad (14)$$

After these preliminaries the ingredients of the torque expression in eqn (5) can readily be expressed in terms of the eccentric anomaly

$$\mathbf{z}\times\mathbf{v} = \sqrt{\mu/a}\,(z_2 s\cos E - z_1\sin E)/(1 - e\cos E)$$
$$\mathbf{z}\times\mathbf{v} = \sqrt{\mu/a}\,\{s\cos E(\mathbf{z}\times\boldsymbol{\eta}_p) - \sin E(\mathbf{z}\times\boldsymbol{\xi}_p)\}/(1 - e\cos E)$$
$$|\mathbf{z}\times\mathbf{v}| = \sqrt{\mu/a}\,f(E)/(1 - e\cos E) \quad (15)$$

with

$$f(E) = \{(s\sin\lambda_p\cos E + \cos\lambda_p\cos\mu_p\sin E)^2 + \sin^2\mu_p\sin^2 E\}^{1/2} \quad (16)$$

The sin E term in the expression for $\mathbf{z}\cdot\mathbf{v}$ indicates that the instantaneous angle of incidence $\lambda(E)$ usually has an asymmetric behaviour around the perigee position.

The complete torque expression of eqn (5) in terms of eccentric anomaly can now be written as

$$\mathbf{M}(E) = -\rho_p(\mu/a)F(E)\{s\cos E(\mathbf{z}\times\boldsymbol{\eta}_p) - \sin E(\mathbf{z}\times\boldsymbol{\xi}_p)\}\exp[-\beta(1 - \cos E)]/(1 - e\cos E)^2 \quad (17)$$

with

$$F(E) = b_0(1 - e^2\cos^2 E)/f(E) + b_1(1 - e^2\cos^2 E)^{1/2} + b_2 f(E) + b_3(z_2 s\cos E - z_1\sin E) \quad (18)$$

3. INTEGRATED ATTITUDE CHANGE OVER PERIGEE REGION

3.1. *Integrated angular momentum change*

The integrated torque over a time interval (t_0, t_1) corresponding the the perigee region crossing equals the cumulative change in satellite angular momentum

$$\Delta\mathbf{H} = \int_{t_0}^{t_1}\mathbf{M}(t)\,dt = (a^3/\mu)^{1/2}\int_{-E_1}^{E_1}\mathbf{M}(E)(1 - e\cos E)\,dE \quad (19)$$

It is important to recognise that odd functions of E in the integrand produce no net contribution after integration over the symmetric interval around perigee. On this basis the *effective* torque expression of eqns (17) and (18) can be simplified to

$$\mathbf{M}(E) = -\rho_p(\mu/a)\{[F_1(E) + F_3(E)]s\cos E(\mathbf{z}\times\boldsymbol{\eta}_p) - [F_2(E) + F_3(E)]\sin E(\mathbf{z}\times\boldsymbol{\xi}_p)\} \times\exp[-\beta(1 - \cos E)]/(1 - e\cos E)^2 \quad (20)$$

with

$$F_1(E) = b_1(1 - e^2\cos^2 E)^{1/2} + b_3 z_2 s\cos E \quad \text{(even)}$$
$$F_2(E) = -b_3 z_1\sin E \quad \text{(odd)}$$
$$F_3(E) = b_0(1 - e^2\cos^2 E)/f(E) + b_2 f(E) \quad \text{(mixed)} \quad (21)$$

The function $F_3(E)$ is the most cumbersome of the three. Since the air density decreases exponentially for E away from zero, it appears reasonable to use expanded versions of $f(E)$ and $1/f(E)$ up to second-order terms of sin E

$$f(E) \cong s\sin\lambda_p\cos E + \cos\lambda_p\cos\mu_p\sin E + \sin^2\mu_p\sin^2 E/(2s\sin\lambda_p)$$
$$1/f(E) \cong \{1 - \cos\mu_p\sin E/(s\tan\lambda_p) + (2\cos^2\lambda_p\cos^2\mu_p - \sin^2\mu_p) \times\sin^2 E/(2s^2\sin^2\lambda_p)\}/(s\sin\lambda_p\cos E) \quad (22)$$

After collecting all contributions the following form for the change in angular momentum is found

$$\Delta\mathbf{H} = -\rho_p\sqrt{\mu a}\,\{I_1(E_1)(\mathbf{z}\times\boldsymbol{\eta}_p) - I_2(E_1)(\mathbf{z}\times\boldsymbol{\xi}_p)\} \quad (23)$$

The integrals $I_j(E_1)$ $(j = 1, 2)$ are defined by

$$I_j(E_1) = \int_{-E_1}^{E_1} G_j(E)\exp[-\beta(1-\cos E)]\,dE \quad (24)$$

where the functions $G_j(E)$ $(j = 1, 2)$ designate those contributions in the torque expression of eqn (20) resulting in even terms in the integrand

$$G_1(E) = [F_1(E) + \{F_3(E)\}_{\text{even}}]s\cos E/(1 - e\cos E)$$
$$G_2(E) = [F_2(E) + \{F_3(E)\}_{\text{odd}}]\sin E/(1 - e\cos E) \quad (25)$$

The even and odd parts of $F_3(E)$ are rather awkward but can readily be derived from eqns (21) and (22) and need not be given here.

The integrals defined in eqn (24) contain a relatively large parameter β, cf. eqn (12), within the exponential. The function $-(1-\cos E)$ reaches its maximum value for $E = 0$, so that the major contribution to the integrals originates from a small region around $E = 0$. Explicit asymptotic approximations for these integrals may be derived by means of the classical Laplace method. The results are in the form of a power-series in terms of $(\beta)^{-1/2-k}$, $k = 0, 1, 2, \ldots$ with validity for large values of β (cf. Appendix)

$$I_j(E_1) \cong \sum_{k=0}^{\infty} \gamma_{jk}(2\pi/\beta^{2k+1})^{1/2}(2k)!/(k!\,2^{2k}) \quad (26)$$

The coefficients γ_{jk} of this asymptotic series correspond to the coefficients of u^{2k} in the power series expansion of

$$G_j(u)/(1 - u^2/2)^{1/2} \quad (j = 1, 2) \quad (27)$$

where $u = (1-\cos E)^{1/2}$. On the basis of the expressions for $G_j(E)$ established above the following results for the leading coefficients can be obtained

$$\gamma_{10} = (1+e)\{b_0/\sin\lambda_p + b_1 + b_2\sin\lambda_p + b_3 z_2\}$$
$$\gamma_{20} = 0$$
$$\gamma_{21} = -2\cos\mu_p\{b_0\cos\lambda_p/\sin^2\lambda_p - b_2\cos\lambda_p + b_3\sin\lambda_p\}/(1-e) \quad (28)$$

The coefficient γ_{11} has also been determined but is omitted here as it is a highly complicated expression.

After substitution of the explicit results for the integrals into eqn (23) the following change in angular momentum is established

$$\Delta\mathbf{H} \cong -\rho_p\sqrt{2\pi\mu H_p/e}\{\gamma_{10}(\mathbf{z}\times\boldsymbol{\eta}_p) + H_p/(2ae)[\gamma_{11}(\mathbf{z}\times\boldsymbol{\eta}_p) - \gamma_{21}(\mathbf{z}\times\boldsymbol{\xi}_p)]\} \quad (29)$$

with an error term of order $\beta^{-5/2}$. It should be noted that the second term is small compared to the main term (by a factor $1/\beta$) so that the angular momentum change is essentially normal to the plane formed by the spin axis and the perigee velocity direction.

3.2. *Geometrical interpretation of attitude change*

The consequence of the result in eqn (29) is that the satellite's spin axis is no longer aligned with the angular momentum vector after perigee passage. For satellites spinning about their major inertia axis the spin axis will eventually align itself with the new angular momentum direction because of energy dissipation effects. On the basis of the leading term of eqn (29) the resulting spin axis attitude direction after perigee passage may be expressed in the form

$$\mathbf{z}^+ \cong \mathbf{z} + \Delta\mathbf{H}/H = (z_1 + \epsilon z_3)\boldsymbol{\xi}_p + z_2\boldsymbol{\eta}_p + (z_3 - \epsilon z_1)\boldsymbol{\zeta}_p \quad (30)$$

with

$$\epsilon = \Delta H/H \cong \rho_p\gamma_{10}\sqrt{2\pi\mu H_p/e}/H \quad (31)$$

This result shows clearly that the spin axis has been rotated over an angle ϵ about the perigee velocity axis $\boldsymbol{\eta}_p$.

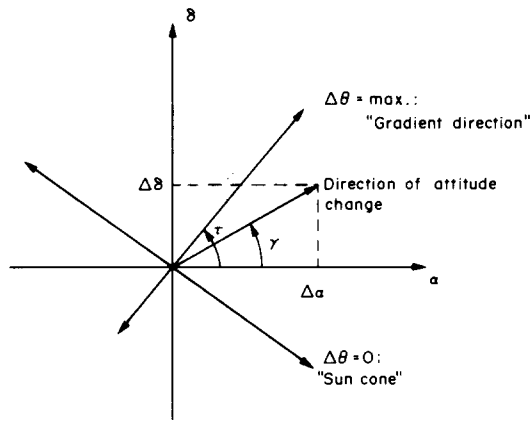

Fig. 6. Geometry of attitude changes in α, δ plane.

The changes in the familiar right ascension α and declination δ of the attitude vector can be obtained after the result of eqn (30) has been transformed to components along the inertial axes. The resulting expressions for $\Delta\alpha$ and $\Delta\delta$ in terms of the orbital elements Ω, ω, i became

$$\Delta\alpha = \epsilon\{\cos\omega\sin i + [\sin\omega\cos(\alpha-\Omega) - \cos\omega\sin(\alpha-\Omega)\cos i]\tan\delta\}$$
$$\Delta\delta = -\epsilon\{\sin\omega\sin(\alpha-\Omega) + \cos\omega\cos(\alpha-\Omega)\cos i\} \quad (32)$$

The angle γ designating the direction of the attitude change in this reference frame follows directly as $\gamma = \arctan(\Delta\delta/\Delta\alpha)$ and is shown in Fig. 6.

The solar aspect angle θ is defined as $\arccos(\mathbf{z}\cdot\mathbf{s})$ where $\mathbf{s}$ is the unit-vector pointing to the sun with components s_j $(j = 1, 2, 3)$ in the inertial reference frame. For small attitude changes the corresponding change in solar aspect angle is represented by

$$\Delta\theta = c_\alpha\Delta\alpha + c_\delta\Delta\delta \quad (33)$$

with

$$c_\alpha = (\partial\theta/\partial\alpha)_{\alpha,\delta} = \cos\delta\,(s_1\sin\alpha - s_2\cos\alpha)/\sin\theta$$
$$c_\delta = (\partial\theta/\partial\delta)_{\alpha,\delta} = \{\sin\delta\,(s_1\cos\alpha + s_2\sin\alpha) - s_3\cos\delta\}/\sin\theta \quad (34)$$

Table 2. Summary of orbital elements and spin vector orientation angles for the three perigees

Perigee	ω	Ω	i	α	δ	λ_p	μ_p
	(degrees)						
1	174.79	273.72	10.565	2.53	−6.35	162.64	−77.16
2	175.14	273.54	10.565	2.48	−6.36	162.68	−77.84
3	175.50	273.36	10.564	3.02	−6.88	162.09	−77.04

The line in the α, δ plane on which $\Delta\theta = 0$ can be interpreted as the (linearised) solar aspect angle cone and may be denoted as $\Delta\delta = -(c_\alpha/c_\delta)\Delta\alpha$. On the other hand, the directions normal to the line $\Delta\theta = 0$ are characterised by the maximum and minimum possible solar aspect angle change and are given by $\Delta\delta = +(c_\delta/c_\alpha)\Delta\alpha$. In the application to be presented hereafter only solar aspect angle measurements are available over the perigee region. Figure 6 shows that if the direction of the predicted attitude change is close to τ or $\tau + \pi$ the observability of the attitude change by means of solar aspect angle measurements is excellent, whereas if γ is near $\tau \pm \pi/2$, the observability is bad.

4. IN-ORBIT VERIFICATION OF THE MODEL

4.1. *Summary of Marecs-A input parameters*

The theory as described above has been applied to the actual conditions valid for ESA's Marecs-A satellite. Table 2 summarises for all three perigee passages the orbital elements Ω, ω and i; the estimates for the spin axis right ascension and declination α, δ as well as the orientation angles λ_p and μ_p (Figs 4 and 5). The predicted air density ρ_p and density scale height H_p will be derived from the standard CNRS 77 model (Barlier *et al.*[4]). Since little variation in solar flux intensity and geomagnetic activity had been observed during the interval of interest, constant values for solar flux $F_{10.7} = 142$; mean solar flux $\overline{F_{10.7}} = 216$ and geomagnetic index $A_p = 6$ will be assumed for the three perigees. A local solar time of 12 h midnight can be taken for all three perigee positions. The geocentric latitude of the three perigee positions was located near 0.9°, whereas the altitude decreased from 199.94 to 199.15 and 198.62 km, respectively. On the basis of these input values the densities and scale heights provided by the CNRS 77 density model are 0.45×10^{-9} kg/m^3 and 33 km, respectively. The altitude dependence of the scale height is ignored in the adopted model [cf. eqns (11) and (12)]. This may be justified on the basis of the exponential decay of the generated torque. The remaining input parameters are taken constant, i.e. eccentricity is 0.730; the angular momentum magnitude is 2412 Nms on the basis of an axial inertia of 352.7 kgm^2 and a spin rate of 65.3 rpm.

4.2 *Predicted attitude and solar aspect angle changes*

Table 3 summarises the predicted variations in right ascension and declination of eqn (32) on the basis of the leading term γ_{10} in the asymptotic series development. The corresponding predicted solar aspect angle changes can be calculated using eqns (33) and (34). The reference solar aspect angles θ for the three perigees follow from the instantaneous sun vector directions and the reference spin vectors as given in Table 2.

The geometrical configuration of the solar aspect angle change appears to be quite favorable. The angle γ indicating the direction of the predicted attitude change is near 193°, whereas the angle $\tau + \pi$ which defines the direction of maximum solar aspect angle decrease in the α, δ plane (Fig. 6) is near 204°. Therefore, the observability of the attitude change by means of solar aspect angle measurements should be excellent in the Marecs-A case.

4.3. *Measured solar aspect angle variations*

The actual evolution of the measured solar aspect angles over the three perigee passages are illustrated in Figs 7–9: the abrupt changes over the perigee times indicated by P_1, P_2 and P_3 are unmistakable. It is not straightforward, however, to identify the magnitude of the changes in an unambiguous manner since they depend on the reference values selected before and after the perigees. In addition, the "natural" solar aspect angle drift due to the apparent sun motion within the adopted inertial frame must be separated from the variation induced by the attitude change.

The adopted procedure is briefly summarised below. The measured solar aspect angles are averaged over batches of 100 measurements collected over about 1.5 min. Obviously false measurements are rejected on the basis of thresholds for the admissible deviation from the expected values. Manoeuvre-free

Table 3. Predicted changes in attitude angles $\Delta\alpha$, $\Delta\delta$ and in solar aspect angle $\Delta\theta$ for the three perigees

Perigee	γ_{10}	$\epsilon \times 10^3$	$\Delta\alpha$	$\Delta\delta$	θ	$\Delta\theta$	c_α	c_δ
			(degrees)					
1	1.428	2.83	−0.047	−0.011	91.170	−0.047	0.910	0.403
2	1.427	2.90	−0.049	−0.011	90.677	−0.049	0.910	0.402
3	1.438	2.98	−0.051	−0.012	90.572	−0.051	0.909	0.402

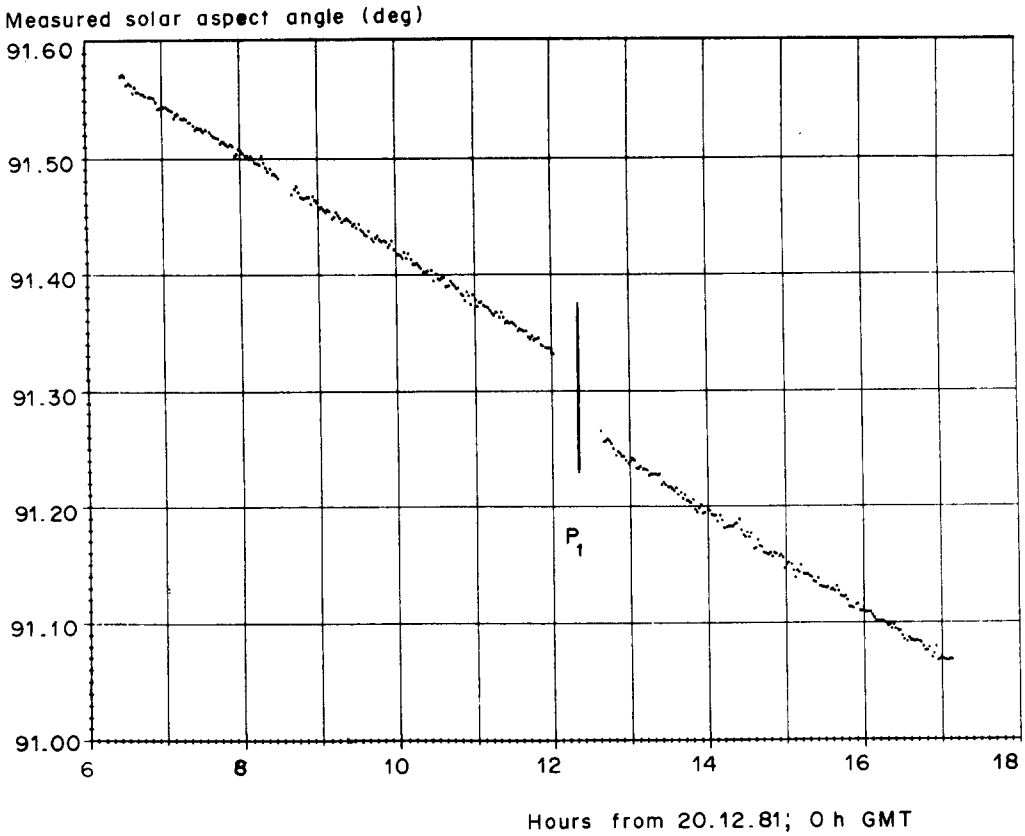

Fig. 7. Measured solar aspect angle evolution over first perigee region of Marecs-A.

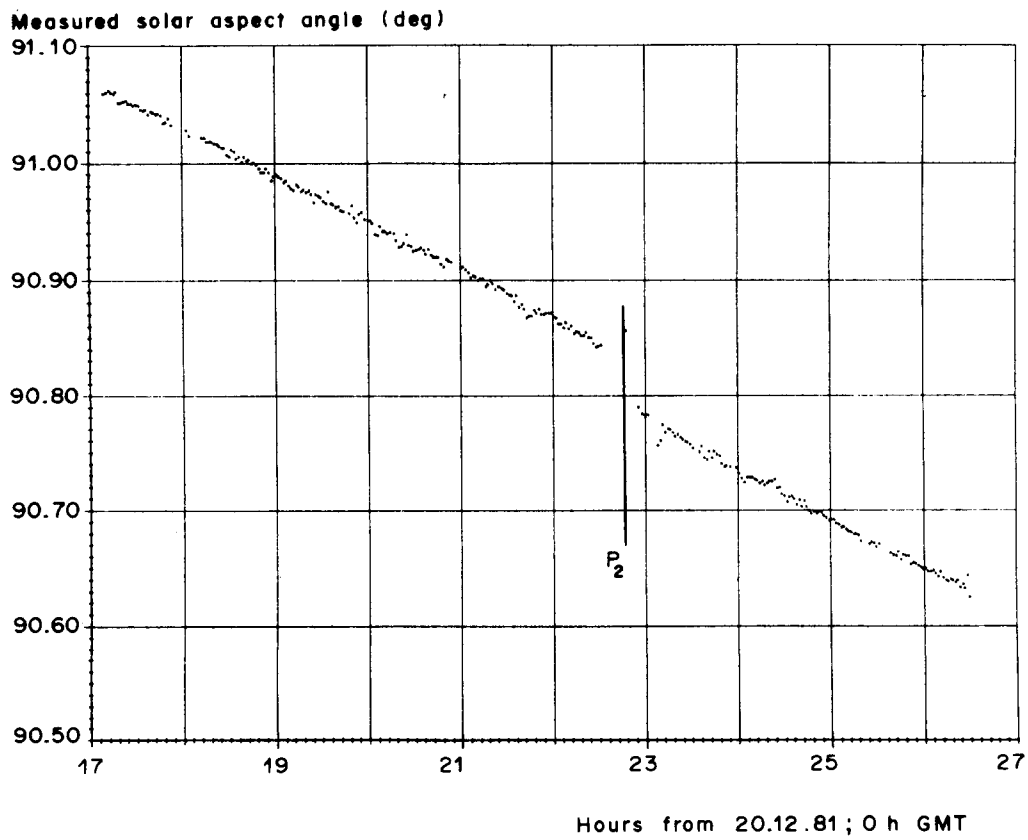

Fig. 8. Measured solar aspect angle evolution over second perigee region of Marecs-A.

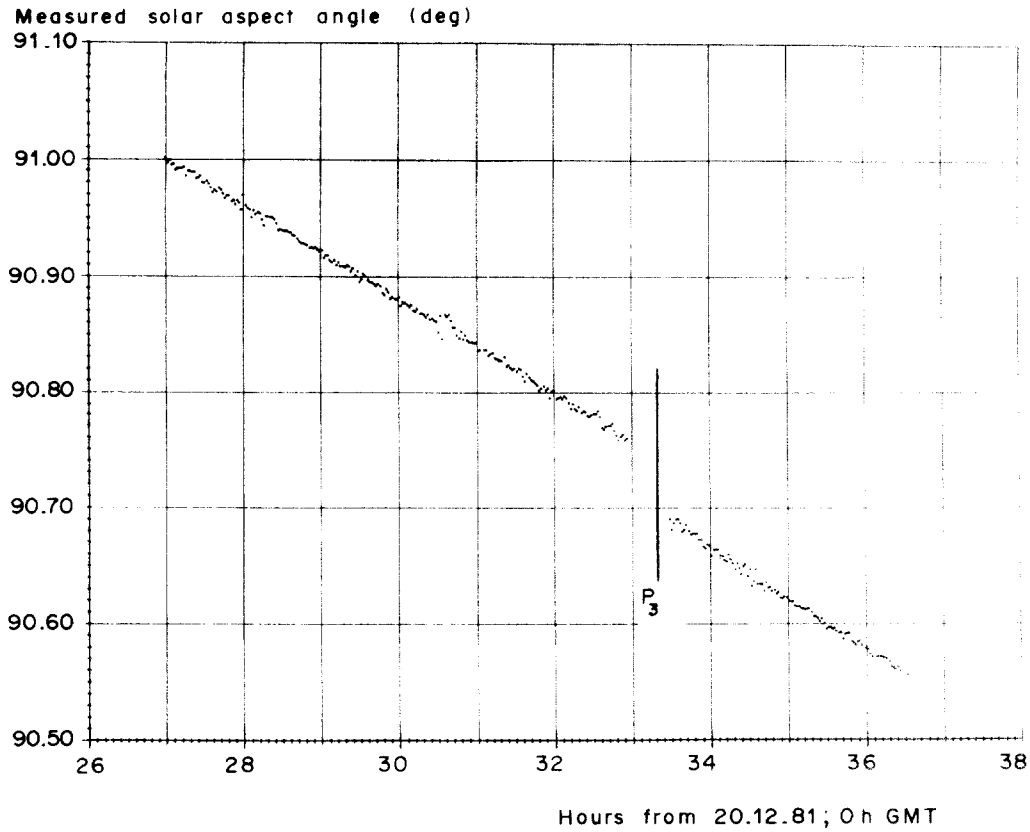

Fig. 9. Measured solar aspect angle over third perigee region of Marecs-A.

intervals are selected before and after each perigee passage. These intervals contain a maximum of 160 and a minimum of 100 averaged measurements. Since the free-molecular torques are negligible at 10 min from perigee the selected intervals should terminate and start at least 10 min before and after perigee passage, respectively. This constraint is automatically satisfied since there is no ground station coverage for about half an hour around perigee.

Subsequently, the natural solar aspect angle drift is calculated for each of the six intervals by means of the formula

$$\dot{\theta}_{\text{nat}} \cong \{(\Delta s_1 \cos\alpha + \Delta s_2 \sin\alpha)\cos\delta + \Delta s_3 \sin\delta\}/(\Delta t \sin\theta) \quad (35)$$

where the vector $\Delta\mathbf{s}$ is evaluated from two sun ephemeris data separated by an interval Δt in the order of 4 h. The reference solar aspect angle θ used here is calculated for the midtime of the interval. A linear regression analysis is applied to the actual solar aspect angle measurements. This results in measured values for the solar aspect angle θ_m at the midtimes as well as measured slopes over each of the six intervals. The values of θ_m may differ from predicted values because of measurement biases and attitude determination errors. Ideally, of course, the slopes found by the regression procedure should be identical to those provided by the natural solar angle drift. In practice, small discrepancies due to measurement imperfections cannot be avoided. The midtime measurements can be estrapolated to the relevant perigee time with the aid of the known natural solar aspect angle drift. The measured solar aspect angle change over perigee follows then from the difference between the extrapolated reference values belonging to the preceding and following intervals.

The results of the regression analysis are summarised in Table 4. It is seen that the maximum error in the reconstituted solar aspect angle rate is 4.5%, but in general the agreement is much better. The 3σ values based on the 99.73% confidence limits for the measured solar aspect angles are below $\pm 0.0009°$ in all cases.

The measured solar aspect angle changes over the perigee region are derived from a comparison of the

Table 4. Natural solar aspect angle drifts and regression results for the six intervals

Mid-time (hr)	$\dot{\theta}_{\text{nat}}$ (deg/hr)	$\dot{\theta}_{\text{meas}}$ (deg/hr)	θ_{meas} (deg)
8.6867	−0.04212	−0.04206	91.4733
14.9827	−0.04212	−0.04237	91.1524
19.5275	−0.04210	−0.04047	90.9665
24.9041	−0.04210	−0.04206	90.6952
30.0280	−0.04204	−0.04014	90.8779
35.1886	−0.04204	−0.04296	90.6118

Table 5. Measured solar aspect angle changes over the three perigees

Perigee	Time (hr)	θ^-_{meas}	θ^+_{meas}	$\Delta\theta_{meas}$ (deg)
1	12.2097	91.3250	91.2692	-0.0558 ± 0.0010
2	22.7286	90.8317	90.7868	-0.0449 ± 0.0011
3	33.2475	90.7426	90.6934	-0.0492 ± 0.0011

measurements extrapolated to the perigee times using the natural drifts of Table 4. Table 5 gives the results as well as the expected 3σ uncertainties in $\Delta\theta_{meas}$ which follow readily from the individual standard deviations in θ_{meas} since the extrapolation does not introduce additional errors. In any case, the error due to the statistical processing of the data is significantly lower than the uncertainty in the air density parameters. When comparing the measured and predicted solar aspect angle changes in Tables 3 and 5 it is seen that the discrepancies range from -16% for the first perigee to $+9\%$ and $+4\%$ in the other perigees.

5. CONCLUDING REMARKS

A mathematical theory for spin axis attitude changes induced by free-molecular torques during the perigee region passage of a geostationary transfer orbit has been constructed. The result is formulated in terms of an asymptotic series with a relatively simple leading term showing that the direction of the attitude change is essentially normal to the plane formed by the attitude orientation and perigee velocity vectors. The model has been verified using actual solar aspect angle measurements collected during the Marecs-A transfer orbit. In this case the observability of the attitude change is excellent as its predicted direction is only 11° away from the direction of maximum solar aspect angle change. By fitting the measurements to a linear curve and subtracting the natural solar aspect angle drift the observed solar aspect angle changes over the three perigee regions have been established. The correspondence with the predictions is -16%, $+9\%$ and $+4\%$ for the three perigees. The differences are expected to be caused by deficiencies in local air density predictions.

The magnitude of the attitude changes has been shown to be of the order of 0.05° for each of the three Marecs-A perigees. It should be noted that this occurred at a time of relatively normal density values: there was no indication of high geomagnetic activity; solar flux values were past their maximum of the 11-year cycle and the local time was near midnight. In this regard it may be of interest to point out that the Japanese CS satellite had its perigee at 156 km and an expected 0.6° attitude change because of free-molecular effects (Iso and Tanaka [5]). Of critical importance to the magnitude of the effect is the air density which would be at its maximum for high solar activity (e.g. during the period 1990–1993), high geomagnetic activity and for local midday times. It is estimated that under such conditions the free-molecular effect on the attitude could be higher by a factor 5 to 10 as compared to the Marecs-A situation. The results of the model presented provide a basis on which a decision can be made concerning the necessity of including these effects in the manoeuvre planning.

REFERENCES

1. J. C. Van der Ha, Evaluation of torques induced by free-molecular flow interaction on spinning satellites (to be published in Journal of the Astronautical Sciences).
2. A. C. Stickland (Editor), *Cospar International Reference Atmosphere (CIRA) 1972.* Akademie-Verlag, Berlin (1972).
3. D. King-Hele, *Theory of Satellite Orbits in an Atmosphere.* Butterworths, London (1964).
4. F. Barlier, C. Berger, L. Falin, G. Kockarts and G. Thuillier, A thermospheric model based on satellite drag data. *Aeronomica Acta A* No. 185, 1–43 (1977).
5. A. Iso and A. Tanaka, Geostationary station acquisition manoeuvres for the "CS" spin-stabilised communication satellite. *Acta Astronautica* **10,** 747–752 (1983).
6. C. M. Bender and S. A. Orszag, *Advanced Mathematical Methods for Scientists and Engineers.* McGraw-Hill, New York (1978).

APPENDIX

Evaluation of integrals $I_j(E_1)$

The generic form of the integrals $I_j(E_1)$ is

$$I(E_1) = \int_{-E_1}^{E_1} g(E) \exp[-\beta(1-\cos E)]\, dE \qquad (A1)$$

with large parameter β and an even function $g(E)$. The Laplace method can be applied after substituting $u = (1-\cos E)^{1/2}$

$$I(u_1) = \sqrt{2} \int_{-u_1}^{u_1} \tilde{g}(u) \exp(-\beta u^2)\, du \qquad (A2)$$

with

$$\tilde{g}(u) = g[E(u)]/(1-u^2/2)^{1/2} \qquad (A3)$$

and $u_1 = u(E_1)$. It is obvious that only the region close to $u = 0$ will contribute significantly to the total integral so that the interval of integration may be extended to ∞. In the neighbourhood of $u = 0$ the (even) function $g(u)$ is expanded in its power series in u

$$\tilde{g}(u) = \sum_{k=0}^{\infty} \gamma_k u^{2k} \qquad (A4)$$

The resulting integral can be solved directly with the aid of the so-called Watson's lemma (e.g. Bender *et al.* [6], p. 263)

$$\Gamma(k+1/2) = \sqrt{\pi}(2k)!/(k!2^{2k}) = \beta^{k+1/2} \int_{-\infty}^{\infty} u^{2k} \exp(-\beta u^2)\, du \qquad (A5)$$

for $k = 0, 1, 2, \ldots$. Comparison of this formula with eqn (A4) produces the desired result

$$I(u_1) \cong \sum_{k=0}^{\infty} \gamma_k (2\pi/\beta^{2k+1})^{1/2} (2k)!/(k!2^{2k}) = \sqrt{2\pi/\beta}\,\{\gamma_0 + \gamma_1/(2\beta) + 3\gamma_2/(4\beta^2) + \cdots\} \qquad (A6)$$